Gas Processing Journal

Vol. 12, No. 1, 2024, pp. 1-16
http://gpj.ui.ac.ir

Research Paper

Numerical Investigation of CO2 Capture from N2-Rich Gas Mixtures Using a Zeolite 13X Packed Bed with Aluminum Foam Heat Transfer Enhancement

Mojtaba Mahdavi Asl [1], Mohammad Hojjat [1*], Mohsen Gholami [1,2]

[1] Department of Chemical Engineering, Faculty of Engineering, University of Isfahan, Isfahan, Iran
[2] Department of Chemical Engineering, Vrije Universiteit Brussel, 1050 Brussels, Belgium

Received: 2026-06-05 Revised: 2026-07-23 Accepted: 2026-08-15

Abstract: A numerical investigation of CO_2 adsorption and desorption in a 13X zeolite packed bed enhanced with aluminum foam for thermal management is presented using a two-dimensional transient model. The rectangular bed (10–30 mm thick) with a 15 mm gas channel is simulated via the finite element method, solving coupled momentum, mass, and energy equations under local thermal equilibrium. Effects of inlet gas velocity, cooling/heating fluid temperatures, and bed thickness on breakthrough, temperature, capacity, desorption, and thermal efficiency are examined with and without foam. Results show that increasing inlet velocity from 0.001 to 0.01 m/s reduces breakthrough time (defined as C_{out}/C_{in}=0.05) from ~300 s to 38 s due to faster saturation. Aluminum foam enhances heat transfer, reducing the time to reach 2.6 mol/kg adsorption capacity in a 30 mm bed from 1995 s to 1540 s (23% reduction). During desorption at 470 K, foam reduces the time for CO_2 loading to drop from 2.72 to 2.38 mol/kg from 1680 s to 1420 s. Higher cooling fluid temperature raises bed temperature and lowers capacity, while higher desorption temperature accelerates regeneration. Thicker beds improve adsorption performance but reduce thermal efficiency due to thermal inertia. Aluminum foam causes a ~5% reduction in thermal efficiency from added thermal mass. Overall, aluminum foam significantly enhances heat transfer and dynamic adsorption performance, demonstrating the potential of foam-enhanced zeolite beds for compact temperature swing CO_2 capture systems.

keywords: Carbon Capture, Aluminum Foam, Zeolite 13X, Adsorption, TSA, Numerical Modeling.

1. Introduction

Notwithstanding the substantial proliferation of renewable energy technologies over recent decades, fossil fuel resources remain fundamentally central to global economic infrastructure. Confronting the imperative to restrict planetary warming to 1.5 °C and attain net-zero carbon dioxide emissions, carbon capture, utilization, and storage (CCUS) has become recognized as an indispensable technological pathway for enabling profound, durable emission abatement. CCUS-based decarbonization can be implemented across four stages-pre-combustion (fuel-derived capture), post-combustion (exhaust gas treatment), oxy-fuel combustion, and direct air capture (ambient air extraction)-each characterized by distinct process advantages and distinct practical deployment constraints [1-4]. Although Direct Air Capture (DAC) provides operational flexibility and can remove legacy emissions, it remains the most expensive CO_2 capture method at \$100–1,000/t CO_2 because CO_2 capture from ambient air is inherently challenging [5]. Post-combustion capture, in contrast, demonstrates superior economic and practical viability at \$47–76/t CO_2, attributable to its foundation in proven unit operations well suited for existing plant retrofits [6]. Pre-combustion, with a cost in the range of \$60–150/t, and oxy-fuel combustion in the range of \$70–160/t face higher costs and complexities related to infrastructure retrofitting or energy demands. While post-combustion remains the most feasible near-term solution, DAC represents a promising long-term

* **Corresponding Author.**
Authors' Email Address: [1] **M. Mahdavi Asl** (mojtaba73.mahdavi.ch@gmail.com), [1] **M. Hojjat** (m.hojjat@eng.ui.ac.ir), [1,2] **M. Gholami** (mohsen.gholami@vub.be)

http://dx.doi.org/10.22108/gpj.2026.149197.1147

pathway for negative emissions [1].

CO_2 capture has been achieved using diverse techniques: absorption, adsorption, cryogenic distillation, membrane separation, chemical looping, and even geothermal or biochemical approaches. The details of these methods, along with their respective advantages, disadvantages, and challenges, have been summarized [7, 8]. Adsorption has emerged as a promising method for carbon dioxide capture and has attracted significant research attention. In this approach, CO_2 is captured using solid adsorbents. Pressure swing adsorption (PSA) and temperature swing adsorption (TSA) are regeneration methods commonly used to restore the adsorption capacity. Owing to the inherently low thermal conductivity of porous solids, conventional TSA processes in packed-bed columns are often limited by the prolonged desorption step, and product purity is also compromised by the use of a regeneration gas. Thus, enhancing heat transfer to the adsorbent seems to be the primary strategy for shortening the desorption time.

One common heat transfer enhancement method in solid adsorbents is the addition of thermally conductive solid particles. These particles, typically metal powders or fillers, are mixed directly with the adsorbent to increase its effective thermal conductivity. By improving heat conduction through the adsorbent bed, this approach can accelerate adsorption/desorption cycles and boost overall system performance. Askalany et al. [9] examined the effect of iron, copper, and aluminum fillers (10–30% by mass) on the thermal conductivity of granular activated carbon. Thermal conductivity increased with metal content. A model of an adsorption cooling system showed that 30% aluminum fillings halved cycle time and doubled specific cooling power. Adding thermally conductive additives (5–25 wt.% of aluminum powder, copper powder, or graphite flakes) to silica-gel-based adsorbent beds was studied by Mika et al. [10]. An increase of up to 20.7% in thermal conductivity was achieved with minimal loss of adsorption capacity. The authors also experimentally examined the regeneration characteristics of zeolite 13X containing metallic additives (aluminum and stainless steel fragments of 1.5–2 cm) and nearly 2 wt.% aluminum oxide nanoparticles [11]. The additions enhanced the desorption rate, with improvements ranging from 19.5% to 22.2%. Straight aluminum pieces increased desorption efficiency by 12.4%, stainless steel by 23.2%, and spiral aluminum pieces by 27.7%. Although the metal additions slightly reduced adsorption capacity, the desorption process was significantly improved.

Another strategy for improving heat transfer is the use of highly porous metal foams or sponges, which act as indirect heat transfer promoters. These metallic structures are often sintered or embedded into the adsorbent bed, creating a continuous conductive pathway that enhances thermal transport from the heat exchanger surface to the adsorbent. This indirect method reduces thermal resistance and allows faster heating or cooling of the adsorbent material. Freni et al. [12] proposed an innovative adsorbent bed design for adsorption chillers. Their approach involved sintering highly porous copper foam directly onto copper tube exteriors, followed by coating the foam with several layers of zeolite 4A using an in situ hydrothermal method. A dynamic model was used to evaluate the bed's performance. Compared with conventional configurations using loose pellets or consolidated zeolite layers, the proposed design exhibits superior specific and volumetric power performance. Mohammed et al. [13] demonstrated that incorporating silica-gel particles into highly porous aluminum foam significantly enhances the effective thermal conductivity of silica-gel/water adsorption beds, resulting in notable improvements in specific cooling power (SCP), volumetric cooling capacity (CP_v), and coefficient of performance (COP). Their combined experimental and numerical investigation evaluated the influence of parameters such as foam pore density (PPI), adsorbent particle diameter, bed thickness, and adsorbent material. The results suggested that aluminum foam with 20 PPI provided the most favorable performance, achieving an SCP of 827 W/kg, a CP_v of 517 W/m^3, and a COP of 0.75.

A highly effective approach to enhance heat and mass transfer is to coat the adsorbent directly onto the surfaces of a heat exchanger. In this configuration, the adsorbent layer is in direct contact with the heat transfer fluid via the heat exchanger walls, minimizing conduction paths and reducing pressure drop. This method, often called an adsorbent-coated heat exchanger, enables rapid temperature swings and efficient utilization of low-grade heat sources. In our previous work, we applied a water-based slurry of zeolite 13X powder and an acrylic latex binder to coat finned tubes. This approach achieved CO_2 desorption within roughly 14 s, which is an order of magnitude faster than any previously documented technique. The adsorbent's working capacity reached approximately 80% of its theoretical maximum, and because only a low regeneration temperature was required, solar energy became a viable heat source. We also observed that raising the adsorbent mass density on the finned tube from 58.5 to 215.7 g/m^2 did not extend the duration of either the adsorption or desorption steps, making it possible to use adsorbent layers as thick as 2.5 mm. Nevertheless, an energy assessment of this indirect heating configuration revealed that its overall energy efficiency remained low [14, 15]. Vannak et al. [16] experimentally investigated a CaA-zeolite-coated adsorber for capturing CO_2 from dry flue gas using low-grade thermal energy within the temperature range of 20–80 °C. Relative to a packed-bed heat exchanger of equivalent volume, the coated adsorber achieved a similar outlet CO_2 concentration and an even greater recovery

efficiency while requiring only about one-third of the adsorbent mass. The study attributed this enhancement to improved heat-transfer characteristics, which promoted faster mass-transfer kinetics. Moreover, extending the gas-flow channel and decreasing the space velocity increased the CO_2 recovery to values above 80%. In contrast, simultaneously increasing the fin spacing and coating thickness, while maintaining a constant adsorbent volume, adversely affected the capture performance because of the thicker adsorbent layer and the reduced gas–solid interfacial area. These observations highlight the critical role of optimizing coating thickness and contact surface area in maximizing the effectiveness of coated heat-exchanger adsorbers. Shaik et al. [17] designed and experimentally evaluated a desiccant-coated heat exchanger (DCHE) operating under an open-cycle configuration. The system utilized ultra-low-grade heat at temperatures of 40–45 °C together with cooling water in the range of 25.4–32.6 °C to satisfy the deep dehumidification and thermal comfort requirements specified by ASHRAE. Experimental results demonstrated that the proposed cycle substantially enhanced the moisture removal capacity (MRC), even when the regeneration temperature was decreased from 50 °C to 40 °C. The study further emphasized that DCHE technology provides an energy-efficient dehumidification strategy, as the cooling medium effectively compensates for the heat released during the sorption process. Zhou et al. [18] proposed a two-stage metal–organic framework coated heat exchanger (MCHE) system. The first stage uses a MOF active at high RH (MIL-101(Cr)), while the second stage employs a MOF suitable for low RH (Al-fumarate), enabling efficient cascade dehumidification across a wide humidity spectrum. Experimental evaluation of key parameters shows that the two-stage configuration outperforms a single-stage setup, delivering a 2–3 °C lower supply air temperature and a 10% increase in dehumidification efficiency. Numerous other studies have also employed these techniques to enhance heat and mass transfer in adsorption systems [19-22].

While metal foams have been studied for adsorption cooling (water vapor), their role in CO_2 capture under temperature swing conditions - especially the coupled heat and mass transfer dynamics as a function of bed thickness and heating/cooling conditions- has not been systematically characterized. Addressing these gaps is essential for the rational design and optimization of high-performance adsorption systems for carbon capture.

In spite of the considerable research devoted to thermally enhanced adsorption systems, significant knowledge gaps remain regarding the application of aluminum foam to CO_2 capture under temperature swing adsorption (TSA) conditions. Most previous investigations of metal-foam-enhanced adsorption systems have focused on water-vapor adsorption for cooling and dehumidification, whereas comparatively few studies have investigated CO_2 capture under TSA conditions. Furthermore, the combined influence of operating variables (heating and cooling temperatures) and structural parameters (bed thickness) on the coupled heat and mass transfer processes governing both adsorption and regeneration has not been comprehensively investigated. In addition, the trade-off between enhanced heat transfer and thermal efficiency has received limited attention.

To address these knowledge gaps, the principal novelty of the present work lies in the development of a two-dimensional transient numerical model that systematically investigates the coupled heat and mass transfer behavior of a zeolite 13X–aluminum foam adsorption bed operating under temperature swing adsorption (TSA) conditions. Unlike previous studies, which have primarily focused on adsorption cooling or isolated operating parameters, the present work provides an integrated assessment of the combined effects of bed geometry and operating temperatures on adsorption performance, breakthrough behavior, regeneration kinetics, and thermal efficiency. The model simultaneously solves the coupled momentum, heat-transfer, mass-transfer, adsorption-equilibrium, and adsorption-kinetics equations. The foam-enhanced configuration is directly compared with a conventional packed bed under identical operating conditions, thereby providing quantitative insight into both the benefits and limitations of aluminum foam. Beyond evaluating thermal enhancement alone, the present study establishes engineering design guidance by quantifying the trade-offs between adsorption performance, regeneration characteristics, and thermal efficiency, which are essential for the design and optimization of compact TSA systems for post-combustion CO_2 capture.

2. Method

2.1. Process and Model Overview

The modeled system (Fig. **1**) comprises a rectangular aluminum foam block, with a length of 250 mm and a variable height of 10 to 30 mm, fully filled with 13X zeolite. Above this foam lies a 15 mm-high channel through which a gas mixture flows at a constant velocity. A separate channel beneath the bed carries a cooling or heating fluid, which removes the heat of adsorption or supplies the heat required for regeneration. The fluid flow rate is assumed high enough that its temperature change along the channel is negligible; consequently, the lower surface of the bed is assigned a fixed temperature. During adsorption, the gas enters the channel at 298.15 K; during desorption, the inlet temperature is 350.15 K.

Error! Reference source not found. lists all relevant properties of the adsorbent, the aluminum foam, and the composite bed.

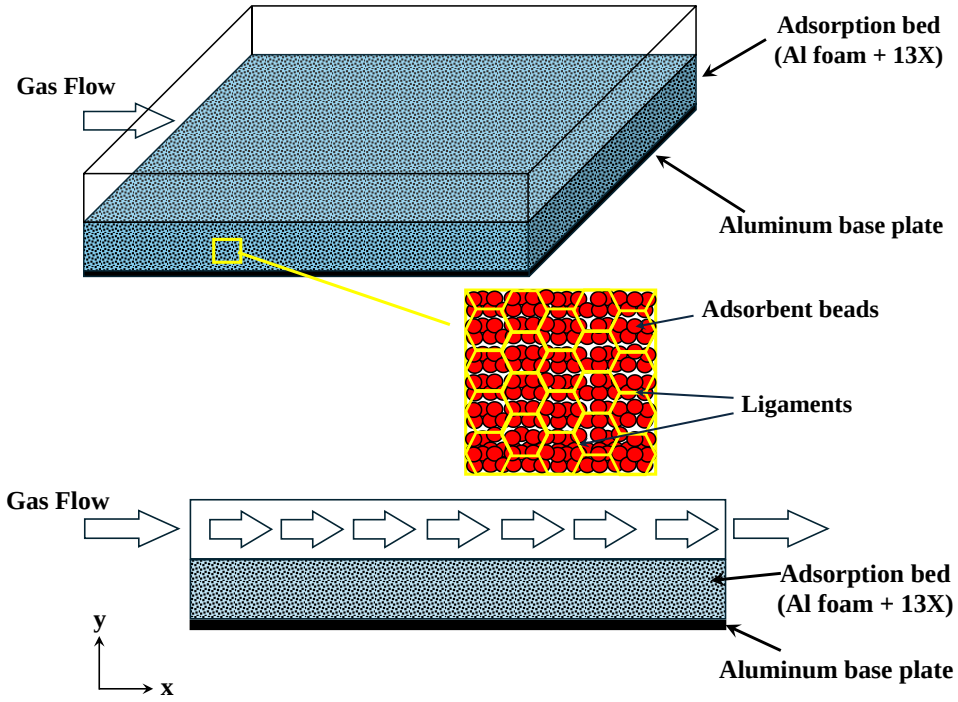

Fig. 1. Geometry of the System

. Thermophysical Properties of the Adsorbent Bed and Aluminum Foam

Property	Value
Particle radius (mm)	1
Particle porosity	0.35
Density (kg m^{-3})	1130
Specific heat (J kg^{-1} K^{-1})	980
Metal foam porosity	0.9
Metal foam density (kg m^{-3})	2700
Total bed porosity	0.42

During adsorption, a gas mixture with a prescribed composition, flow velocity, and temperature enters the gas channel and then passes across the channel–bed interface into the adsorbent bed. Once inside the porous adsorbent, the gas components transfer to the adsorbent surface, where uptake occurs. After the adsorbent reaches saturation and the adsorption phase ends, the system switches to desorption. In this regeneration phase, the temperatures of both the heating fluid and the incoming gas mixture are increased, causing the previously captured components to be released from the adsorbent.

2.2. Governing Equations

The model was formulated based on the following simplifying assumptions:

• The system is represented as a two-dimensional, time-dependent problem.

• Mass transfer between the gas and solid phases is described using a linear driving force (LDF) approach.

• The gas phase is assumed to behave as an ideal gas.

• Fluid flow in the channel is considered to be in the creeping (Stokes) flow regime.

• Adsorption equilibrium is modeled using a dual-site Langmuir isotherm.

• The aluminum foam matrix and zeolite adsorbent are treated as a single pseudo-homogeneous solid phase.

The continuity equation for the gas phase in the free-flow region (gas channel) is expressed as follows:

$$\frac{\partial}{\partial t}(\rho_g) + \nabla \cdot (\rho_g u) = 0 \quad (1)$$

The following equation represents the mass conservation within the gas channel and applies to both configurations with and without the presence of metal foam.

$$\frac{\partial w_{1,i}}{\partial t} + \nabla \cdot (u w_{1,i}) = \nabla \cdot (D_{M,i} \nabla w_{1,i}) \quad (2)$$

Here, $w_{1,i}$ denotes the concentration of species i, while $D_{M,i}$ represents the molecular diffusivity of species i, expressed in m^2/s.

The mass conservation equation for the adsorbent layer is expressed as follows:

$$\frac{\partial}{\partial t}(\varepsilon_t w_{2,i}) + \rho_s f_{am}(1-\varepsilon_t)\frac{\partial q_i}{\partial t} = \nabla \cdot (D_{g,i} \nabla w_{2,i}) \quad (3)$$

where, $w_{2,i}$ denotes the i^{th} component concentration in the porous bed gas phase in mol/m^3, $\varepsilon_t$represents the total bed porosity, and f_{am} is the mass fraction of adsorbent material within the bed. The transport coefficients are defined as $D_{g,i}$ for the effective gas-phase diffusivity of component i in m^2/s. Finally, q_i is the total loading of component i on the adsorbent, given in mol/kg.

The assumption of local thermal equilibrium (LTE) in adsorption process modeling has been widely adopted and validated for porous adsorption systems operating under moderate gas

velocities and exhibiting efficient internal heat transfer [13, 23]. In the present configuration, the relatively low gas velocities together with the high thermal conductivity of the aluminum foam promote rapid heat exchange between the gas, adsorbent particles, and metallic matrix, thereby minimizing local temperature differences and supporting the LTE assumption. Consequently, the aluminum foam and zeolite adsorbent are represented as a pseudo-homogeneous solid phase characterized by effective thermophysical properties.

It should be noted, however, that this approximation may become less accurate under conditions involving significantly higher gas velocities, rapid thermal transients, or larger characteristic dimensions, where local thermal non-equilibrium (LTNE) between the gas, adsorbent particles, and metallic foam may develop. In such cases, separate energy equations for the gas and solid phases would be required to resolve interphase temperature differences. Therefore, the present model is most applicable to compact TSA systems operating within the investigated range of operating conditions. Based on these assumptions, the energy conservation equation for the adsorbent-filled aluminum foam bed is written as follows:

$$\left(\varepsilon_t\rho_g C_{pg} + (1-\varepsilon_f)\rho_f C_{pf} + (1-\varepsilon_t)\rho_s\left(C_{ps} + \sum_i q_i C_{p,i}\right)\right)\frac{\partial T_b}{\partial t} = \nabla\cdot(k_b\nabla T_b) + (1-\varepsilon_t)\rho_s\sum_i \Delta H_{ai}\frac{\partial q_i}{\partial t} \quad (4)$$

Here, ρ_f is the density of the aluminum foam (kg m^{-3}), $C_{p,f}$ is the specific heat capacity of the aluminum foam (J kg^{-1} K^{-1}), and ε_t is the total porosity of the bed, ρ_g (kg m^{-3}) is density of the fluid, $C_{p,g}$ (J kg^{-1} K^{-1}) is specific heat capacity of the fluid, ρ_s is the solid adsorbent density (kg m^{-3}), k_b is the effective thermal conductivity of the bed and is taken as 6 $Wm^{-1}K^{-1}$ [13], and ΔH_{ai} is the heat of adsorption of species i (kJ kg^{-1}), T_b is the mean bed temperature (K), and q_i is the amount of species i adsorbed per unit mass of adsorbent.

The coefficient of the first term on the left-hand side of the equation represents the total heat capacity of the bed. The first term on the right-hand side corresponds to thermal diffusion, while the second term on the right-hand side accounts for the energy generated or consumed during the adsorption and desorption processes.

The energy conservation equation for the gas phase within the channel is given as follows:

$$\rho_g C_{p,g}\frac{\partial T_g}{\partial t} + \rho_g C_{p,g}u.\nabla T_g = \nabla\cdot\left(k_g\nabla T_g\right) \quad (5)$$

$C_{p,g}$ is the gas-phase specific heat in J kg^{-1} K^{-1}, ρ_g is the fluid density in kg m^{-3}, T_g is the gas temperature in K, and k_g is the gas thermal conductivity in $Wm^{-1}K^{-1}$.

The energy conservation equation in the adsorbent layer, without aluminum foam, is given by the following equation:

$$\left(\varepsilon_t\rho_g C_{p,g}+(1-\varepsilon_t)\rho_s\left(C_{p,s}+\sum_i q_i C_{p,i}\right)\right)\frac{\partial T_b}{\partial t} = (1-\varepsilon_t)\rho_s\sum_i \Delta H_{a,i}\frac{\partial q_i}{\partial t}+\nabla\cdot(k_b\nabla T_b) \quad (6)$$

The left-hand side term of the equation, characterized by its coefficient, represents the aggregate thermal capacity of the bed. On the right-hand side, the first term represents the enthalpy change associated with the adsorption–desorption cycle, accounting for the heat released or absorbed during the process. The second term describes heat conduction within the system.

The primary parameter that differentiates the cases with and without metallic foam in the mass conservation formulation is the overall bed porosity, ε_t. This parameter governs the effective void fraction of the adsorption bed and is defined as [13]:

$$\varepsilon_t = \varepsilon_b + (1-\varepsilon_b)\varepsilon_p \quad (7)$$

$$\varepsilon_b = 1 - \frac{m_{ad}}{(1-\varepsilon_p)\rho_s V\varepsilon_{fo}} \quad (8)$$

ε_t is the bed total porosity, ε_b is the porosity of the bed, ε_p is the adsorbent porosity, and ε_{fo} is the foam porosity (For the case without metal foam, ε_{fo} is taken as 1), m_{ad} is the mass of the adsorbent (kg), and V is the total volume of the bed (m^3).

The gas flow in the channel is governed by the continuity equation (1) and the momentum equation for creeping flow (Stokes equation):

$$\rho_g\frac{\partial u}{\partial t} = \nabla\cdot[-pI+\tau] \quad (9)$$

In the above, τ is the viscous stress tensor for a compressible Newtonian fluid. Given that viscosity is a function of temperature, the stress tensor is expressed as:

$$\tau = \mu(T)(\nabla u + (\nabla u)^T) - \frac{2}{3}\mu(T)(\nabla\cdot u)I \quad (10)$$

In these equations, ρ_g is the gas density (kg/m^3), u is the velocity vector (m/s), p is the pressure (Pa), T is the temperature (K), μ is the dynamic viscosity (Pa·s), and superscript T denotes the transpose operation. The gas density ρ_g is evaluated using the ideal gas law, while the temperature field is obtained from the solution of the energy conservation equation.

In the porous adsorbent bed, the flow is described by Darcy's law:

$$u_D = -\frac{K}{\mu_g}\nabla P \quad (11)$$

where K is the permeability of the bed (m^2).

2.3. Heat Transfer and Mass Transfer Parameters

To determine the equilibrium adsorption values, the dual-site Langmuir isotherm was employed,

which is given by the following equation [24]:

$$q_i^e = \frac{q_{s1,i} b_i w_{1,i}}{1 + \sum b_i w_{1,i}} + \frac{q_{s2,i} d_i w_{1,i}}{1 + \sum d_i w_{1,i}} \quad (12)$$

$$b_i = b_{s01} \exp\left(-\frac{E_{1,i}}{RT}\right) \quad (13)$$

$$d_i = b_{s02} \exp\left(-\frac{E_{2,i}}{RT}\right) \quad (14)$$

The values of the parameters in these equations are provided in Table 1 [24].

Table 1. Parameters of the Dual-Site Langmuir Isotherm [24]

Component	E_1 J mol^{-1}	E_2 J mol^{-1}	b_{s01} mol m^{-3}	b_{s02} mol m^{-3}	q_{s1} mmol g^{-1}	q_{s2} mmol g^{-1}
CO_2	-36641.21	-35690.66	8.65×10^{-7}	2.63×10^{-8}	3.09	2.54
N_2	-15800	0.00	2.50×10^{-6}	0.00	5.84	0.00

Adsorption kinetics are described by the Linear Driving Force (LDF) model, as expressed by Equation (15) [25].

$$\frac{dq_i}{dt} = k_{LDF,i}(q_{e,i} - q_i) \quad (15)$$

where $k_{LDF,i}$ is the mass transfer coefficient:

$$k_{LDF,i} = \frac{15 D_{e,i}}{r_p^2} \quad (16)$$

The effective diffusivity of component i is calculated by [25]:

$$D_{e,i} = \frac{\epsilon_p}{\tau_p} \frac{D_{K,i} D_M}{D_{K,i} + D_M} \quad (17)$$

$D_{K,i}$ and D_M are the Knudsen diffusion coefficient of component i and the molecular diffusion coefficient, respectively [25]:

$$D_{K,i} = 48.5 D_{pore} \sqrt{\frac{T}{M_i}} \quad (18)$$

$$D_M = \frac{0.01 T^{1.75} \sqrt{\frac{M_{N_2} + M_{CO_2}}{M_{N_2} M_{CO_2}}}}{P\left(Dv_{N_2}^{1/3} + Dv_{CO_2}^{1/3}\right)^2} \quad (19)$$

The properties of the gas mixture are computed based on the correlations provided in Table 2.

Table 2. Correlations Used for Calculating the Thermophysical Properties of the Gas Mixture

Heat capacity	$C_{pg} = \sum_{i=1}^{n} y_i C_{p.i}$	(20)
Heat capacity of component i [26]	$C_{p.i}/R = A_0 + A_1 T + A_2 T^2 + A_3 T^3 + A_4 T^4$ Constant values are provided in Table 3	(21)
Density	$\rho_g = \frac{P \sum_{i=1}^{n} y_i M_i}{1000 RT}$	(22)
Thermal conductivity [26]	$k_g = \sum_{i=1}^{n} \frac{y_i k_i}{\sum_{j=1}^{n} y_i \phi_{ij}}$	(23)
	$\phi_{ij} = \left[8\left(1 + \frac{M_i}{M_j}\right)\right]^{-\frac{1}{2}} \left[1 + \sqrt{\frac{\mu_i}{\mu_j}} \left(\frac{M_j}{M_i}\right)^{\frac{1}{4}}\right]^2$ and $\phi_{ji} = \frac{\mu_j}{\mu_i} \frac{M_i}{M_j} \phi_{ij}$	(24)
Viscosity of component i [26]	$\mu_i = 2.669 \times 10^{-6} \frac{(M_i T)^{0.5}}{\sigma_i^2 \Omega_\mu}$	(25)
	$\sigma_{CO_2} = 3.941$ and $\sigma_{N_2} = 3.798$ Å	
	$\Omega_\mu = A(T^*)^{-B} + C\exp(-DT^*) + E\exp(-FT^*)$	(26)
	$T^* = kT/\varepsilon$	(27)
	A=1.16145, B=0.14874, C=0.52487, D=0.77320, E=2.16178, F=2.43787	
Viscosity of gas mixture [26]	$\mu_g = \sum_{i=1}^{n} \frac{y_i \mu_i}{\sum_{j=1}^{n} y_i \phi_{ij}}$	(28)

Table 3. Constants of Heat Capacity Equation [26]

Component	A_0	$A_1\times10^3$	$A_2\times10^5$	$A_3\times10^8$	$A_4\times10^{11}$
CO_2	3.259	1.356	1.502	-2.347	1.056
N_2	3.539	-0.261	0.007	0.157	-0.099

The thermal efficiency of the system is defined as the ratio of the heat consumed for desorption of the adsorbed components to the total heat input to the system during the desorption stage, and is computed by the following equation:

$$\eta_{th} = \frac{Q_{des}}{Q_{tot}} \times 100 \quad (29)$$

where Q_{tot} denotes the total heat input to the system, and Q_{des} represents the heat consumed for desorption of the adsorbed components, and is expressed by the following equation:

$$Q_{des} = m_{ad} \sum_{i=1}^{n} \left(q_i \Delta H_{des,i} M_i\right) / 1000 \quad (30)$$

$$\Delta H_{des,i} = -RT^2 \left(\frac{\partial \ln P_i}{\partial T}\right)_{\theta_i} \quad (31)$$

$$\theta_i = \frac{q_i}{q_i^e} \quad (32)$$

The total heat input to the system is calculated as:

$$Q_{tot} = Q_w + Q_{des} \quad (33)$$

where Q_w is the amount of energy transferred to the metal foam and adsorbent.

$$Q_w = (mC_p\Delta T)_{adsorbent} + (mC_p\Delta T)_{foam} \quad (34)$$

2.4. Initial and Boundary Conditions

According to Fig. 2, initial and boundary conditions are listed in Table 4. The breakthrough time was defined as the time at which the outlet CO_2 concentration reached 5% of the inlet concentration (i.e., C_{out}/C_{in}=0.05). Unless otherwise stated, this criterion was used throughout the manuscript for all breakthrough-time comparisons.

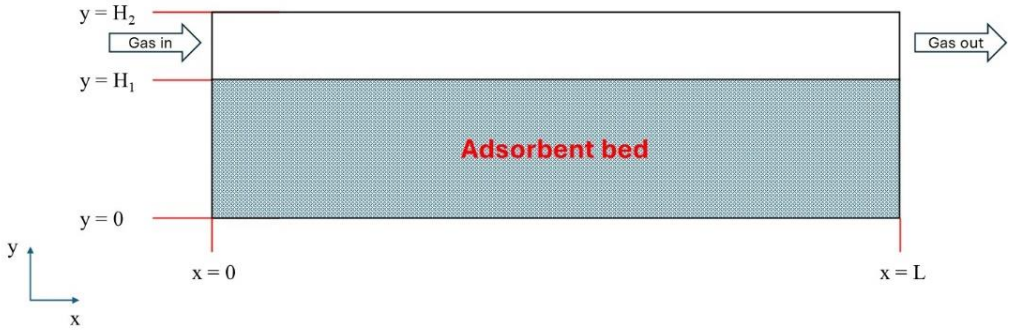

Fig. 2. Two-Dimensional Geometry of the System

Table 4. Initial and Boundary Conditions

Initial temperature	t = 0	T_i = 298.15 K
Adsorbent initial loading	t = 0	$w_{i,initial}$ = 0
Adsorption temperature	y = 0, 0 < x < L	T_{ad}
Desorption temperature	y = 0, 0 < x < L	T_{des}
Gas inlet concentration	x = 0, H_1 < y < H_2	C_0 = 40 mol m^{-3}
Gas inlet velocity	x = 0, H_1 < y < H_2	u_0
Channel outlet	x = L, H_1 < y < H_2	P = P_{atm}
Heat transfer boundary conditions at channel inlet and outlet	x = 0 and x = L	$\frac{\partial T}{\partial x} = 0$
Heat transfer boundary conditions at upper surface of the channel	y = H_2	$\frac{\partial T}{\partial y} = 0$
Heat transfer boundary conditions at gas/adsorbent interface	y = H_1	$k_b \frac{\partial T_b}{\partial n} = k_g \frac{\partial T_g}{\partial n}$
Mass transfer boundary conditions at channel inlet and outlet	x = 0 and x = L	$\frac{\partial w_{1,i}}{\partial x} = 0$
Mass transfer boundary conditions at channel lower surface	y = 0	$\frac{\partial w_{2,i}}{\partial y} = 0$
Mass transfer boundary conditions at channel upper surface	y = H_2	$\frac{\partial w_{1,i}}{\partial y} = 0$
Mass transfer boundary conditions at gas/adsorbent interface	y = H_1	$D_{g,i} \frac{\partial w_{2,i}}{\partial n} = D_M \frac{\partial w_{1,i}}{\partial n}$

2.5. Solution Method

The governing equations were solved numerically using the finite element method. The computational domain was discretized into a structured grid, and the weak form of each equation was implemented. A backward differentiation formula (BDF) scheme with adaptive time stepping was employed for temporal discretization to ensure stability and accuracy. The strong coupling between mass and energy balances was handled iteratively at each time step using a Picard iteration technique, with convergence declared when the relative residuals fell below 10-6.

Although the present model captures the principal transport phenomena governing adsorption and regeneration, several simplifying assumptions should be recognized. The pseudo-homogeneous representation neglects pore-scale temperature gradients within the adsorbent particles and aluminum foam, while the LTE assumption assumes instantaneous thermal equilibration among the constituent phases. Furthermore, the model neglects thermal contact resistance between the foam and adsorbent, possible radiation heat transfer at elevated temperatures, and any changes in adsorbent properties during repeated adsorption-desorption

cycles. These simplifications reduce computational cost while preserving the dominant physics of the system under investigation. Nevertheless, future work could employ local thermal non-equilibrium (LTNE) formulations and pore-scale simulations to investigate the conditions under which these assumptions may no longer hold.

3. Results and Discussion

For the purpose of validating the simulation, the results obtained were compared with those reported by Mohammed et al. [13]. The mass of water vapor adsorbed per unit mass of adsorbent as a function of time in the foam-adsorbent bed is presented in Fig. 3, while the average bed temperature as a function of time is shown in Fig. 4. The very good agreement between the present simulation results and those of Mohammed et al. [13] confirms the validity of the simulation. For the amount of water vapor adsorbed per unit mass of adsorbent, the maximum and average deviations between the present study and the findings of Mohammed et al. are 5% and 2.5%, respectively. For the average bed temperature, the corresponding differences are 1.2% and 0.5%.

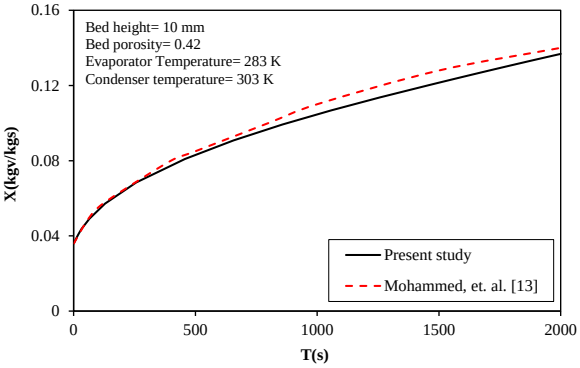

Fig. 3. The Adsorbed Mass of Water Vapor per Unit Mass of Adsorbent in the Foam-Adsorbent Bed as a Function of Time

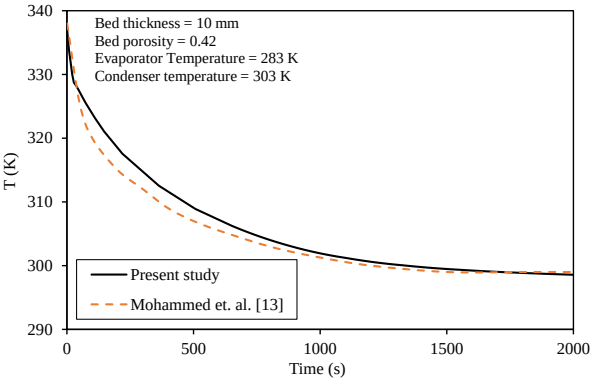

Fig. 4. The Average Bed Temperature as a Function of Time

To assess mesh independence, the effect of mesh size variations using triangular mesh elements was investigated for three cases: a coarse mesh with 5,297 elements, a finer mesh with 11,062 elements, and an extra fine mesh with 36,432 elements. The breakthrough curve was compared and analyzed at a constant inlet velocity of 0.001 m/s and a constant inlet temperature of 298.15 K, in order to select the simplest mesh configuration that provides acceptable results in solving the equations. A comparison of these three cases indicated no noticeable difference due to mesh size, as illustrated in Fig. 5. Therefore, the coarse mesh was assumed to simplify the solution of the equations.

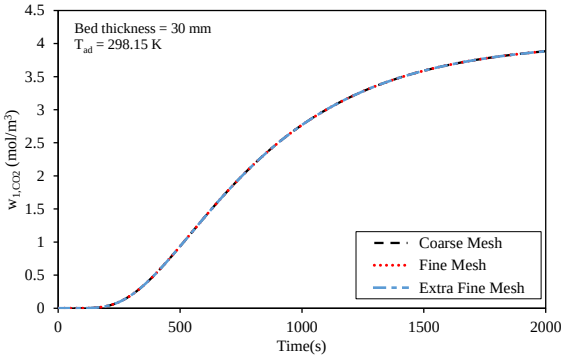

Fig. 5. Effect of Mesh Size on the Breakthrough Curve

The breakthrough curves of CO_2 at different inlet gas velocities are presented in Fig. **6**. The breakthrough time reported throughout this work corresponds to an outlet concentration ratio of C_{out}/C_{in}=0.05. It is observed that increasing the inlet gas velocity causes the outlet CO_2 concentration to reach its inlet value more rapidly.

At a velocity of 0.01 m/s, it takes only 38 seconds for the mass transfer zone front to reach the outlet of the duct, whereas at a velocity of 0.001 m/s, this time increases to 300 seconds. The inlet temperature and the adsorption step temperature were assumed constant at 298.15 K. The inlet composition of the gas mixture was 90% nitrogen and 10% carbon dioxide in all cases.

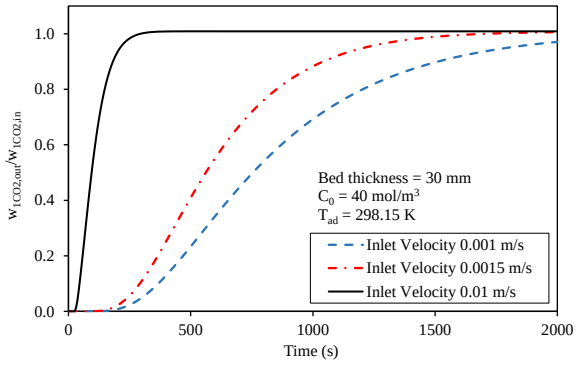

Fig. 6. Effect of Inlet Gas Velocity on the CO_2 Breakthrough Curve

An increase in inlet gas velocity exerts two concomitant effects on the dynamic behavior of a fixed-bed adsorber, both of which contribute to a reduction in breakthrough time. First, the higher gas velocity results in an increased mass loading rate, meaning a greater quantity of adsorbate is

introduced into the bed per unit time. Given that the adsorbent possesses a finite capacity, this accelerated input rate leads to faster saturation of the available sites, thereby causing the mass transfer zone (MTZ) to traverse the column more rapidly and reach the outlet sooner. Second, elevating the gas velocity has a dual impact on mass transfer kinetics. On the one hand, it reduces the external mass transfer resistance, which is beneficial for adsorption kinetics. On the other hand, it significantly shortens the residence time of the gas within the bed. This reduced contact time limits the period available for the adsorbate to diffuse into the adsorbent particles. It is important to note that the intra-particle diffusion process itself occurs at its own intrinsic rate and is not directly hindered by the gas velocity; however, the shorter residence time means that the adsorbate has less time to penetrate the particles before the gas exits the bed. Consequently, the mass transfer zone becomes broader or more elongated, indicating less efficient utilization of the bed, as a larger portion of the bed remains partially unsaturated at the point of breakthrough. This decreased efficiency further accelerates the appearance of the adsorbate in the effluent. Thus, the observed decrease in breakthrough time at higher velocities is attributable to both the increased rate of adsorbate delivery and the reduced bed utilization efficiency caused by the limited time available for intra-particle diffusion.

The breakthrough behavior also reflects the strong coupling between convective mass transport and the thermal characteristics of the adsorption bed. Because CO_2 adsorption on zeolite 13X is exothermic, rapid adsorption near the bed inlet produces localized temperature rises that reduce the equilibrium adsorption capacity. At higher inlet velocities, the increased CO_2 loading rate intensifies this localized heat generation while simultaneously shortening the time available for heat dissipation into the aluminum foam and the cooling boundary. Consequently, both thermal and concentration gradients become steeper, causing the mass-transfer zone to propagate more rapidly through the bed. This interaction between adsorption kinetics, heat generation, and convective transport explains why breakthrough occurs substantially earlier than would be expected from residence-time considerations alone.

The effect of the cooling fluid temperature during the adsorption step on system performance was investigated at three adsorption temperatures: 300, 310, and 315 K. The inlet gas temperature was set at 298.15 K, and the inlet gas velocity was held constant at 0.001 m/s. The thicknesses of the bed and the channel were also assumed to be constant. The average bed temperature as a function of time is shown in Fig. 7. Increasing the cooling fluid temperature leads to an increase in the average bed temperature. Furthermore, the figure demonstrates that in the absence of foam, the bed temperature rise is significantly larger, which is attributed to the low thermal conductivity of the bed. This indicates that the presence of the metal foam enhances the heat transfer rate and improves the controllability of the bed temperature by the cooling fluid.

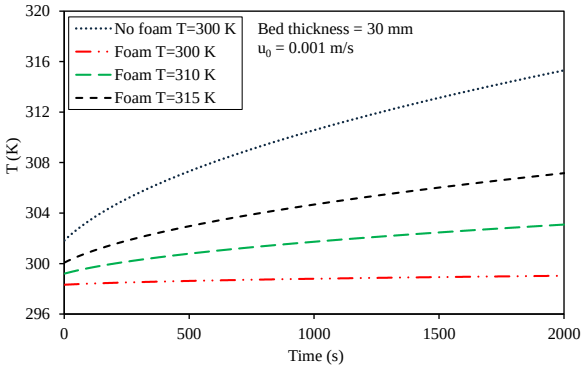

Fig. 7. Average Bed Temperature with Time at Different Cooling-Water Temperatures during the Adsorption Step

The average amount of CO_2 adsorbed on the bed as a function of time at different adsorption temperatures is shown in Fig. 8. As the cooling water temperature increases, the average adsorption capacity of the bed decreases, which is attributed to the corresponding rise in bed temperature. Furthermore, a comparison of the two curves corresponding to the cases with and without aluminum foam at a given cooling water temperature reveals that the presence of foam significantly enhances the adsorption capacity. This improvement is a direct consequence of more efficient heat transfer and the resulting reduction in the average bed temperature.

The observed reduction in adsorption capacity is governed by the coupled interaction between heat transfer and adsorption equilibrium. The adsorption of CO_2 on zeolite 13X is an exothermic process; therefore, any increase in bed temperature shifts the equilibrium toward lower CO_2 loading according to the dual-site Langmuir isotherm. Aluminum foam improves thermal conductivity throughout the bed, allowing the heat released during adsorption to be dissipated more rapidly toward the cooling surface. As a result, the bed remains closer to isothermal conditions, preserving a larger thermodynamic driving force for adsorption while simultaneously maintaining favorable conditions for intraparticle diffusion.

Thus, the improvement associated with aluminum foam arises not only from faster heat removal but also from its indirect enhancement of adsorption equilibrium and mass-transfer effectiveness.

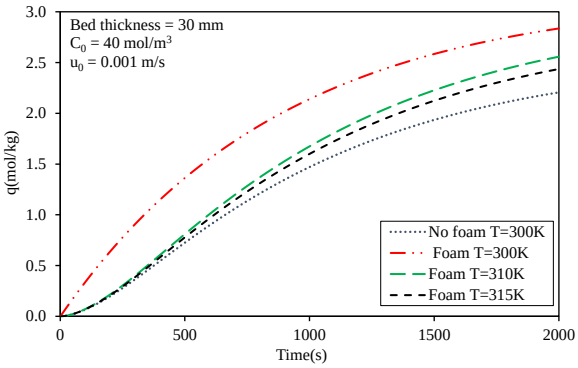

Fig. 8: Average Amount of CO_2 Adsorbed Over Time at Different Cooling-Water Temperatures in the Adsorption Step

To investigate the effect of bed thickness on the average bed temperature and adsorption capacity over time, the system was simulated at three bed thicknesses of 10, 20, and 30 mm. The average bed temperature as a function of time is shown in Fig. 9. The inlet gas temperature was set at 298.15 K, the adsorption stage temperature was 298.15 K, the inlet gas velocity was 0.001 m/s, and the gas channel thickness was fixed at 15 mm. Increasing the bed thickness introduces two competing physical effects. On one hand, the larger quantity of adsorbent and aluminum foam increases the thermal mass of the system, thereby damping temperature fluctuations generated by the exothermic adsorption process. On the other hand, the greater distance between the cooling surface and the upper regions of the bed increases the conductive heat-transfer path and thermal resistance. Within the range of bed thicknesses investigated in this study, the beneficial influence of the increased thermal mass dominates, resulting in a lower average bed temperature.

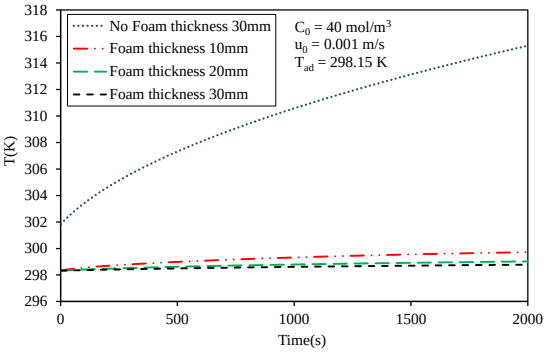

Fig. 9. The Average Temperature of the Adsorbent Bed Over Time for Different Bed Thicknesses

The average adsorption capacity of the bed as a function of time for different bed thicknesses (10, 20, and 30 mm) is presented in Fig. 10. The inlet gas temperature was set at 298.15 K, the adsorption stage temperature was 298.15 K, the inlet gas velocity was 0.001 m/s, and the gas channel thickness was fixed at 15 mm. As observed, increasing the bed thickness leads to an increase in adsorption capacity due to the corresponding decrease in the average bed temperature. Furthermore, the presence of metal foam reduces the adsorption time. For instance, the addition of metal foam reduces the time required for the adsorption capacity to reach 2.6 mol/kg in a 30 mm thick bed from 1995 seconds to 1540 seconds, corresponding to a reduction of approximately 23%.

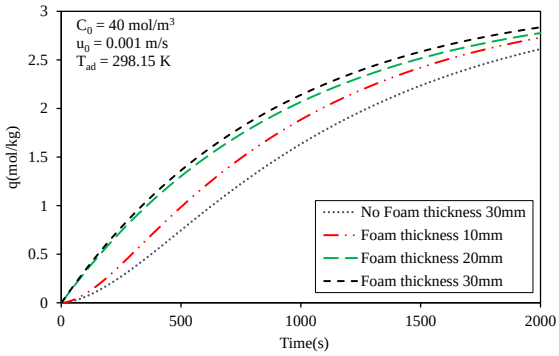

Fig. 10. The Effect of Bed Thickness on the Adsorption Capacity Over Time

The increase in adsorption capacity observed for thicker beds is therefore not solely a consequence of the larger amount of adsorbent. The lower average bed temperature maintains a higher equilibrium loading while the larger thermal inertia suppresses rapid temperature excursions during adsorption. These two mechanisms collectively improve utilization of the adsorbent inventory. Nevertheless, excessively thick beds may eventually become limited by internal heat-transfer resistance, suggesting that an optimum bed thickness is expected beyond the range investigated in the present study.

The final conditions of the adsorption step were taken as the initial conditions for the desorption step. The inlet gas velocity was maintained constant at 0.001 m/s. The inlet gas temperature was increased to 350.15 K. The system performance was investigated for three different desorption temperatures-430, 450, and 470 K- and three adsorbent and foam (bed) thicknesses of 10, 20, and 30 mm. In all cases, the gas channel height was fixed at 15 mm.

The effect of the heating fluid temperature during the desorption step is illustrated in Fig. 11. The bed height was fixed at 30 mm. Increasing the desorption step temperature resulted in a higher average bed temperature. Additionally, in the absence of foam and the resulting lack of adequate

thermal conduction, the average bed temperature was lower.

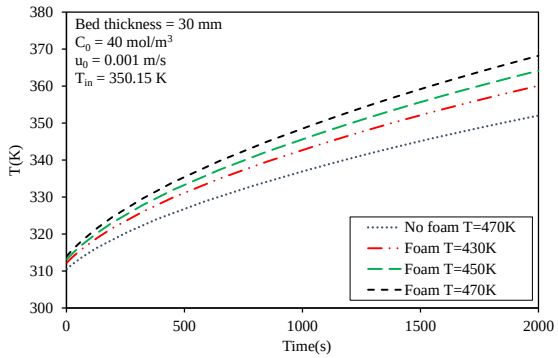

Fig. 11. The Effect of the Heating Fluid Temperature on the Average Bed Temperature during the Desorption Process

The average amount of adsorption as a function of time at different heating fluid temperatures during the desorption stage is shown in Fig. 12. It is observed that increasing the desorption step temperature reduces the average adsorption capacity of the bed because of the increase in bed temperature, which indicates an increase in the amount desorbed. Naturally, since the desorption process is endothermic, elevating the temperature favors desorption and enhances the amount desorbed. Furthermore, it is observed that due to the improved conductive heat transfer within the bed, the desorption time is significantly reduced in the presence of aluminum foam. For instance, with the addition of aluminum foam, the time required to reduce the adsorbed carbon dioxide loading from 2.72 mol/kg to 2.38 mol/kg at a heating fluid temperature of 470 K decreases from 1680 seconds to 1420 seconds.

Desorption performance is governed simultaneously by heat-transfer rate and adsorption equilibrium. Increasing the heating-fluid temperature not only accelerates heat penetration into the bed but also shifts the adsorption equilibrium toward lower CO_2 loading, thereby increasing the thermodynamic driving force for desorption. Aluminum foam substantially reduces conductive resistance within the bed, allowing this equilibrium shift to occur more uniformly throughout the adsorbent. Consequently, regeneration becomes more spatially uniform, reducing the time required to reach the target residual loading.

The effect of bed thickness at three levels of 10, 20, and 30 mm on the average bed temperature and adsorption capacity was investigated. Fig. 13 presents the average bed temperature as a function of time for different bed thicknesses. The figure shows that increasing the bed thickness reduces the average bed temperature, which is attributed to the increased mass of adsorbent and metal foam, as well as the greater thermal resistance of the bed.

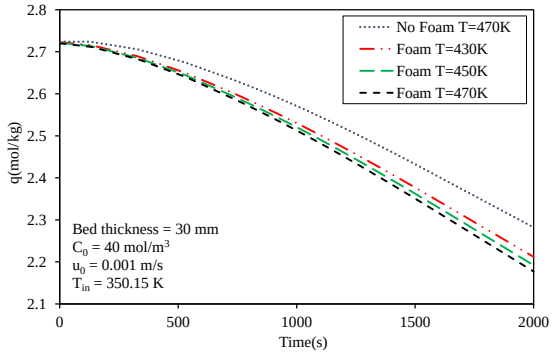

Fig. 12. Average CO_2 Loading as a Function of Time at Different Heating-Fluid Temperatures during the Desorption Step

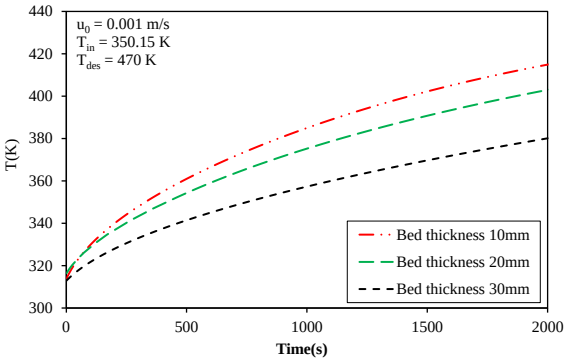

Fig. 13. The Effect of Adsorbent and Foam Thickness on the Average Temperature of the Bed during the Desorption Process

The average amount of carbon dioxide adsorbed by the bed as a function of time for different bed thicknesses is shown in Fig. 14. It is evident that increasing the bed thickness leads to an increase in the average adsorption capacity of the bed. This is attributed to the reduction in the average bed temperature. Since the desorption process is endothermic, a decrease in bed temperature does not favor desorption and consequently reduces the average amount of desorbed mass from the bed.

Unlike the adsorption stage, increasing the bed thickness during desorption introduces a greater thermal penalty because additional thermal energy is required to heat both the adsorbent and the aluminum foam. Although thicker beds contain more adsorbent, the increased thermal inertia delays the establishment of the high temperatures required for effective regeneration. Consequently, thermal transport rather than adsorption equilibrium becomes the dominant limitation for thick beds during the early stages of desorption.

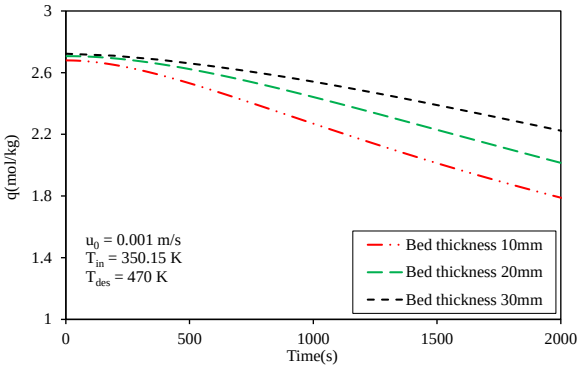

Fig. 14. The Effect of Bed Thickness on the Average Amount of Carbon Dioxide Adsorbed by the Bed in the Desorption Step

The thermal efficiency of the system was calculated for the cases with and without foam. The results indicate a 5% decrease in efficiency when foam is present in the bed. The reduction in thermal efficiency originates from the additional sensible heat stored within the aluminum foam during regeneration. Although the foam markedly enhances conductive heat transfer and shortens adsorption/desorption cycles, part of the supplied thermal energy is consumed in increasing the temperature of the metallic matrix instead of directly contributing to CO_2 desorption. This illustrates a fundamental engineering trade-off in thermally enhanced adsorption systems: increasing thermal conductivity improves dynamic process performance but simultaneously increases the thermal mass that must be heated during each regeneration cycle. These results are presented in Fig. 15.

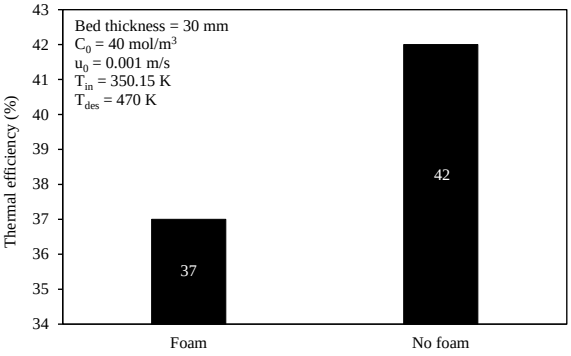

Fig. 15. Comparison of the Thermal Efficiency of the System with and without the Presence of Aluminum Foam

Additionally, the thermal efficiency was investigated for three different bed thicknesses of the foam and adsorbent of 15, 20, and 25 mm. Increasing the bed thickness reduces the thermal efficiency of the system due to the corresponding increase in bed mass. These results are presented in Fig. 16.

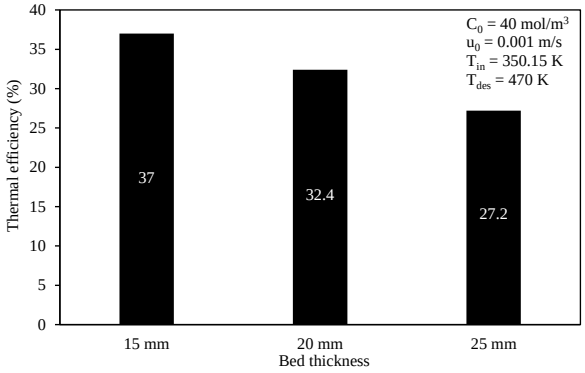

Fig. 16. The Effect of Bed Thickness on the Thermal Efficiency of the System

These results suggest that the optimal design of foam-enhanced TSA systems should not maximize thermal conductivity alone. Instead, an appropriate balance must be established between thermal conductivity, adsorbent inventory, and thermal inertia in order to maximize overall process performance. Consequently, future optimization studies should simultaneously consider cycle time, adsorption capacity, regeneration efficiency, and energy consumption rather than treating these objectives independently.

3.1. Engineering Implications

The numerical results obtained in this study have several implications for the practical design of temperature swing adsorption (TSA) systems for post-combustion CO_2 capture. The simulated feed gas, containing 10% CO_2 and 90% N_2, represents the composition of many industrial flue gases, including those generated by natural gas-fired power plants and several industrial heating processes. Therefore, the trends identified in the present work are directly relevant to practical carbon capture applications employing low-pressure adsorption systems.

The results demonstrate that aluminum foam significantly enhances heat transport within the adsorption bed, thereby reducing both adsorption and regeneration times. Faster thermal response shortens the overall cycle time, which can increase process productivity and potentially reduce the required adsorbent inventory for a given CO_2 capture capacity. Such improvements are particularly attractive for compact adsorption units where equipment size and cycle time are important economic considerations.

However, the simulations also reveal an important engineering trade-off. Although aluminum foam accelerates heat transfer, its relatively high heat capacity introduces an additional sensible heat requirement during regeneration. Consequently, part of the supplied thermal energy is consumed in heating the metallic matrix rather than directly providing the heat of desorption. In the present study, this effect resulted in an approximately 5% reduction in

thermal efficiency, despite the substantial improvements in adsorption and regeneration kinetics. Therefore, the selection of aluminum foam should not be based solely on maximizing thermal conductivity. Instead, the optimum foam configuration should be determined by simultaneously considering thermal conductivity, regeneration energy, cycle time, productivity, and overall process economics.

Another important design consideration is the selection of bed thickness. Increasing the bed thickness enhances adsorption capacity because of the larger adsorbent inventory and the lower average bed temperature during adsorption. However, thicker beds also increase thermal inertia, resulting in longer heating periods during regeneration and a corresponding reduction in thermal efficiency. Consequently, the optimal bed geometry should balance adsorption capacity, regeneration time, equipment size, and energy consumption rather than maximizing any single performance indicator.

Although the present study focuses on the behavior of a single adsorption bed, the observed trends provide useful guidance for the design of industrial multi-bed TSA systems. In practical installations, the reduction in cycle time achieved by enhanced heat transfer may translate into higher throughput and smaller adsorption units, partially compensating for the modest increase in regeneration energy associated with the aluminum foam. A complete techno-economic assessment, however, requires system-level optimization considering cyclic operation, heat recovery, pressure losses, auxiliary equipment, and operating costs. Such analyses are beyond the scope of the present work but represent an important direction for future research.

4. Conclusions

A parallel-channel system consisting of an aluminum foam matrix packed with Zeolite 13X adsorbent was numerically simulated for the capture of carbon dioxide from a gas mixture containing 10% CO_2 and 90% N_2. The flow rate, temperature, and composition of the inlet gas, the height of the gas channel, and the porosity of the aluminum foam were held constant. The effects of the cooling fluid temperature during the adsorption stage, the bed thickness, and the heating fluid temperature during the desorption stage on system performance were investigated.

The results show that increasing the cooling fluid temperature raises the average bed temperature during adsorption and reduces the CO_2 uptake capacity of the adsorbent. During desorption, a higher heating fluid temperature likewise increases the average bed temperature, thereby enhancing the amount desorbed. Increasing the bed thickness during adsorption leads to a lower average bed temperature and a higher CO_2 adsorption capacity. Conversely, increasing the bed thickness during desorption reduces the average bed temperature, which corresponds to a lower amount desorbed and a less favorable system performance.

The incorporation of aluminum foam improves heat transfer, resulting in a lower average bed temperature during adsorption and a higher equilibrium CO_2 adsorption capacity. In addition, the enhanced thermal conductivity accelerates both adsorption and regeneration kinetics, reducing the time required to reach a specified adsorption loading by approximately 23% and shortening the desorption time by approximately 15.5%.

The thermal efficiency of the system is slightly reduced when metallic foam is used, because a portion of the heat supplied during desorption is consumed in raising the temperature of the foam itself. Thermal efficiency also decreases with increasing bed thickness, due to both the reduced desorption capacity (caused by lower bed temperatures) and the increased mass of adsorbent and foam. Overall, the inclusion of aluminum foam improves the dynamic performance of the adsorption system by increasing the effective CO_2 adsorption capacity during the adsorption step and accelerating both adsorption and desorption kinetics. However, this improvement is accompanied by a modest reduction in thermal efficiency because of the additional sensible heat required to heat the metallic foam during regeneration.

From an engineering perspective, the results demonstrate that the modest reduction in thermal efficiency is outweighed by the substantial reduction in adsorption and regeneration times, making aluminum foam an attractive option for compact TSA systems where high productivity is a primary design objective. Nevertheless, the improved dynamic performance is accompanied by a modest increase in sensible heat demand due to the thermal mass of the foam. Therefore, the design of foam-enhanced adsorption beds should simultaneously consider equilibrium adsorption capacity, adsorption and regeneration kinetics (cycle time), and regeneration energy requirements to achieve an optimal balance between productivity and energy efficiency.

Overall, the present results demonstrate that aluminum foam provides an effective strategy for intensifying heat transfer in compact TSA systems and can substantially improve process productivity when appropriately balanced against regeneration energy requirements.

References

[1] I. F. Elegbeleye, O. A. Oguntona, F. A. Elegbeleye, The role of Carbon Capture, Utilization, and Storage (CCUS) technologies and Artificial Intelligence (AI) in achieving net-zero carbon footprint: Advances, implementation challenges, and future perspectives, Technologies. 13(11) (2025) 509. https://doi.org/10.3390/technologies13110509.

[2] IEA, World Energy Outlook 2025, Paris. (2025). https://www.iea.org/reports/world-energy-outlook-2025

[3] S. Mazhar, M. W. Mumtaz, M. El Oirdi, H. Mukhtar, M. A. Raza, M. Farhan, M. Aatif, G. Muteeb, Synergizing advanced materials and artificial intelligence for next-generation carbon capture, utilization, and storage (CCUS): A review, RSC Advances. 16(3) (2026) 2621-2651. https://doi.org/10.1039/d5ra07338c.

[4] A. Nema, A. Kumar, V. Warudkar, An in-depth critical review of different carbon capture techniques: Assessing their effectiveness and role in reducing climate change emissions, Energy Conversion and Management. 323 (2025) 119244. https://doi.org/10.1016/j.enconman.2024.119244.

[5] G. Realmonte, L. Drouet, A. Gambhir, J. Glynn, A. Hawkes, A. C. Köberle, M. Tavoni, An inter-model assessment of the role of direct air capture in deep mitigation pathways, Nature Communications. 10(1) (2019) 3277. https://doi.org/10.1038/s41467-019-10842-5.

[6] W. J. Schmelz, G. Hochman, K. G. Miller, Total cost of carbon capture and storage implemented at a regional scale: Northeastern and midwestern United States, Interface Focus. 10(5) (2020). https://doi.org/10.1098/rsfs.2019.0065.

[7] M. Bui, C. S. Adjiman, A. Bardow, E. J. Anthony, A. Boston, S. Brown, P. S. Fennell, S. Fuss, A. Galindo, L. A. Hackett, J. P. Hallett, H. J. Herzog, G. Jackson, J. Kemper, S. Krevor, G. C. Maitland, M. Matuszewski, I. S. Metcalfe, C. Petit, G. Puxty, J. Reimer, D. M. Reiner, E. S. Rubin, S. A. Scott, N. Shah, B. Smit, J. P. M. Trusler, P. Webley, J. Wilcox, N. Mac Dowell, Carbon capture and storage (CCS): The way forward, Energy & Environmental Science. 11(5) (2018) 1062-1176. https://doi.org/10.1039/c7ee02342a.

[8] T. A. Saleh, Nanomaterials and hybrid nanocomposites for CO_2 capture and utilization: Environmental and energy sustainability, RSC Advances. 12(37) (2022) 23869-23888. https://doi.org/10.1039/d2ra03242b.

[9] A. A. Askalany, S. K. Henninger, M. Ghazy, B. B. Saha, Effect of improving thermal conductivity of the adsorbent on performance of adsorption cooling system, Applied Thermal Engineering. 110 (2017) 695-702. https://doi.org/10.1016/j.applthermaleng.2016.08.075.

[10] Ł. Mika, T. Bujok, K. Sztekler, W. Kalawa, E. Radomska, A. Mlonka-Mędrala, J. Čespiva, P. Boruta, Development of new composite beds for enhancing the heat transfer in adsorption cooling systems, Energies. 18(3) (2025) 584. https://doi.org/10.3390/en18030584.

[11] M. Sidhareddy, S. Tiwari, Experimental investigation for enhancement of heat and mass transfer during regeneration of zeolite 13X-water pair, International Journal of Refrigeration. 159 (2024) 297-308. https://doi.org/10.1016/j.ijrefrig.2023.12.041.

[12] A. Freni, L. Bonaccorsi, E. Proverbio, G. Maggio, G. Restuccia, Zeolite synthesised on copper foam for adsorption chillers: A mathematical model, Microporous and Mesoporous Materials. 120(3) (2009) 402-409. https://doi.org/10.1016/j.micromeso.2008.12.011.

[13] R. H. Mohammed, O. Mesalhy, M. Abdelkareem, L. C. Chow, Performance enhancement of adsorption beds with silica-gel particles packed in aluminum foams, International Journal of Refrigeration. 104 (2019) 201-212. https://doi.org/10.1016/j.ijrefrig.2019.03.013.

[14] F. Esmaeili, M. Gholami, M. Hojjat, Accelerated CO_2 capture on adsorbent coated finned tube: An experimental study, Energy. 187 (2019) 116014. https://doi.org/10.1016/j.energy.2019.116014.

[15] F. Esmaeili, M. Hojjat, J. F.M. Denayer, M. Gholami, CO2 capture on an adsorbent-coated finned tube heat exchanger: Effect of the adsorbent thickness, Industrial & Engineering Chemistry Research. 60 (2021) 4677−4681. https://doi.org/10.1021/acs.iecr.0c06171.

[16] H. Vannak, Y. Osaka, T. Tsujiguchi, A. Kodama, Zeolite-coated fin–coil heat exchanger for CO_2 recovery from simulated dry flue gas via low-temperature-heat-driven TSA, Sep. Purif. Technol. 325 (2023) 124688. https://doi.org/10.1016/j.seppur.2023.124688.

[17] G. A. Shaik, V. Prabakaran, M. K. Jagirdar, Deep dehumidification using novel cycle-operated desiccant-coated heat exchangers driven by an ultra-low-grade heat source, Energy Conversion and Management. 349 (2026) 120836. https://doi.org/10.1016/j.enconman.2025.120836.

[18] X. Zhou, Y. Feng, L. Ge, Z. Su, T. Ge, Two-stage MOF-coated heat exchanger for efficient humidity control under wide humidity range, Energy Conversion and Management. 348 (2026) 120726. https://doi.org/10.1016/j.enconman.2025.120726.

[19] X. Q. Duong, N. V. Cao, W. S. Lee, M. Y. Park, J. D. Chung, K. J. Bae, O. K. Kwon, Effect of coating thickness, binder and cycle time in adsorption cooling applications, Applied Thermal Engineering. 184 (2021) 116265. https://doi.org/10.1016/j.applthermaleng.2020.116265.

[20] M. Z. Liu, W. D. Chen, Y. L. Shao, Z. F. Huang, Z. Y. Zeng, Y. D. Wan, K. J. Chua, Experimental analysis and investigation of desiccant coated heat exchanger applications involving condensation and sorption mechanisms, Energy. 305 (2024) 132255. https://doi.org/10.1016/j.energy.2024.132255.

[21] J. Liu, C. Sun, Q. Chen, Experimental study of desiccant-coated heat exchangers for deep dehumidification, Energy and Buildings. 319 (2024) 114554.

https://doi.org/10.1016/j.enbuild.2024.114554.
[22] S.-Y. Woo, K.-H. Kim, J.-S. Kim, Y.-D. Kim, Development and performance evaluation of novel silica gel-coated heat exchanger with high durability and conductivity to improve adsorption water treatment, Desalination. 563 (2023) 116720. https://doi.org/10.1016/j.desal.2023.116720.
[23] İ. Solmuş, D. Andrew S. Rees, C. Yamalı, D. Baker, A two-energy equation model for dynamic heat and mass transfer in an adsorbent bed using silica gel/water pair, International Journal of Heat and Mass Transfer. 55(19) (2012) 5275-5288. https://doi.org/10.1016/j.ijheatmasstransfer.2012.05.036.
[24] R. Haghpanah, A. Majumder, R. Nilam, A. Rajendran, S. Farooq, I. A. Karimi, M. Amanullah, Multiobjective optimization of a four-step adsorption process for postcombustion CO2 capture via finite volume simulation, Industrial & Engineering Chemistry Research. 52(11) (2013) 4249-4265. https://doi.org/10.1021/ie302658y.
[25] D. Ko, R. Siriwardane, L. T. Biegler, Optimization of pressure swing adsorption and fractionated vacuum pressure swing adsorption processes for CO2 capture, Industrial & Engineering Chemistry Research. 44(21) (2005) 8084-8094. https://doi.org/10.1021/ie050012z.
[26] B. E. Poling, J. M. Prausnitz, J. P. O'Connell, The properties of gases and liquids, 5th ed., McGraw-Hill, New York. (2001). https://www.accessengineeringlibrary.com/content/book/9780070116825.